Soft Decision Viterbi Decoder for FSK Demodulation Under Fast Fading Channel

Daisuke NOJIMA*, Yuhei NAGAO*, Masayuki KUROSAKI*, Hiroshi OCHI*,
Akira ISHIKAWA†, Shugo FUKAGAWA† and Akihiro TAHIRA†
*Faculty of Computer Science and Systems Eng., Kyushu Institute of Technology
680-4 Kawazu Iizuka-shi Fukuoka-ken 820-8502, JAPAN
Email: {nojima, nagao, kurosaki, ochi}@dsp.cse.kyutech.ac.jp
†R&D Division, Kyushu TEN
2360 Yunokimoto-machi Sasebo-shi Nagasaki-ken 857-0115, JAPAN
Email: {a-ishikawa, s-fukagawa, a-tahira}@qten.co.jp

***Abstract*—In a soft decision Viterbi decoder, the log-likelihood ratio (LLR) metric is used to improve the performance of the error correction. However, this cannot be directly applied in frequency shift keying (FSK) wireless transmission system which uses a frequency discriminator for FSK de-modulation - an inherently non-linear circuit. The LLR for a linear system cannot be used for the FSK wireless transmission system. It is necessary to calculate LLR which considers the non-linear characteristic of the frequency discriminator. In this paper, we derive the modified LLR which considers the non-linear characteristic of the frequency discriminator. Simulation shows the effectiveness of the derived LLR for 4-ary FSK wireless transmission system.**

I. Introduction

Recently, in order to further improve the quality of communication and reduce manufacturing cost, wireless communication is adopting digital modulation to replace analog modulation. For example, frequency modulation (FM) - an analog modulation scheme used in the terrestrial mobile communication is modified to frequency shift keying (FSK) - a digital modulation scheme [1].

Wireless systems are known to suffer from several wireless propagation effects like multipath and Doppler shift. Without proper mitigation, error occurs in the received signal.

Generally, the mechanisms which correct these errors are the convolutional encoder found in the transmitter and the soft decision Viterbi decoder in the receiver [2]. In the soft decision Viterbi decoder, a log-likelihood ratio (LLR) metric is used to improve the ability of the error correction as opposed to the hard decision Viterbi decoder. Currently, these systems assume a linear system such that the noise statistics at the input of the decoder are linearly tractable. Since an FSK wireless transmission system uses an inherently non-linear frequency discriminator for FSK demodulation [3], it is because necessary to modify the LLR to take into account the non-linear characteristic of the frequency discriminator. For example, an FSK modulation system was proposed in [4] using a Viterbi decoder; however, it was not soft decision. In this paper, we numerically reformulate the LLR suitable for the non-linear characteristic of the frequency discriminator. Simulation results show the effectiveness of the derived LLR for 4-ary FSK wireless transmission system.

II. System Outline

Figure 1 shows the transmitter architecture. Table I lists the symbol mapping for this system. After symbol mapping, the data is oversampled using a period T_u and band limitation is done with the root-roll-off filter. The resulting baseband signal after filtering is represented as $s(t)$. The FSK modulation is done by shifting the frequency of the numerically controlled oscillator (NCO) according to the baseband signal $s(t)$.

TABLE I
Symbol Mapping for FSK Wireless System

Symbol	Bit Information
3	01
1	00
-1	10
-3	11

Finally, the baseband signal $s(t)$ after FSK modulation is then transmitted. As for the Additive White Gaussian Noise (AWGN) channel, the noise $n(t)$ in-phase and quadrature components are Gaussian distributed with zero mean and variance $\sigma^2/2$.

In the receiver, FSK de-modulation is done by a frequency discriminator. Figure 2 shows the receiver architecture. The frequency discriminator converts from rectangular coordinate to polar coordinate using the $\arctan$ circuit in order to extract the phase information from the received signal. From here on, we concentrate on the phase error $\phi(t)$ via small signal analysis caused by the noise $n(t)$. This $\phi(t)$ is passed to a differentiator which transforms $\phi(t)$ to the frequency error. Note that the sampling rate at this point is still the oversampled rate T_u. This is because that the receiver root-roll-off filter is last performed in this FSK system. Also, note that the change in phase information per unit time is equivalent to the frequency information. Finally, the frequency error $e(t)$ can now be calculated from the phase error $\phi(t)$.

III. Probability Distribution

A. Phase Error

In this part, the probability density function of the phase error $\phi(t)$ from the output of the $\arctan$ circuit in the

978-1-4244-7057-0/10/$26.00 ©2010 IEEE

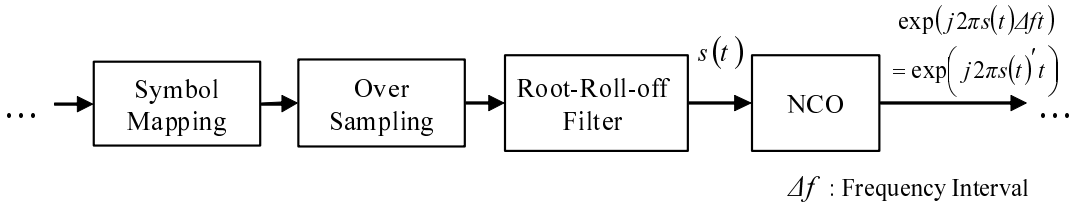

Fig. 1. Transmitter Architecture

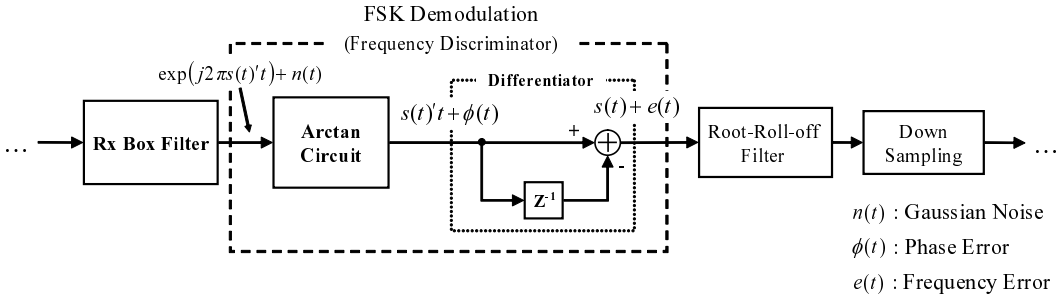

Fig. 2. Receiver Architecture

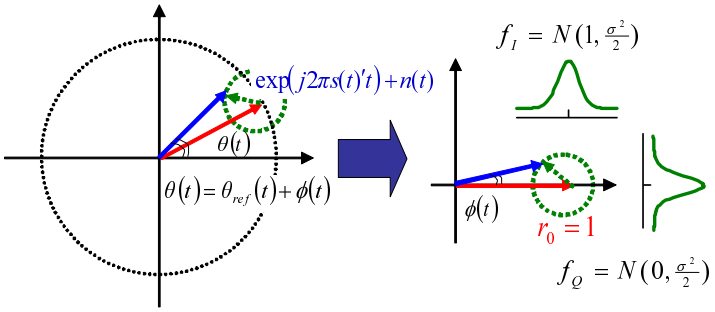

Fig. 3. Received Signal Model

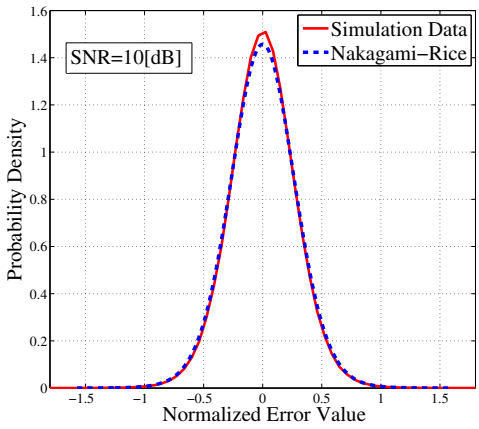

Fig. 4. Comparison of Simulation Data with Nakagami-Rice Distribution (SNR = 10 [dB])

frequency discriminator is explained.

Assuming that the transmitted signal amplitude is unity as shown in Fig.3, we model the phase error $\phi(t)$ distribution as a Nakagami-Rice distribution based on prior simulation data. As shown in Fig.4, the Nakagami-Rice model fits well with the distribution of simulated $\phi(t)$ data. The Nakagami-Rice distribution $f(\phi)$ is shown in eq.(1) [5][6].

$$\begin{aligned} f(\phi) &= \frac{1}{2\pi}\exp\left(-\frac{1}{2\sigma^2}\right)\left[1+\sqrt{\frac{\pi}{2}}\frac{\cos\phi}{\sigma}\exp\left(\frac{\cos^2\phi}{2\sigma^2}\right)\cdot\right. \\ &\quad \left.\left\{1+\mathrm{erf}\left(\frac{\cos\phi}{\sqrt{2}\sigma}\right)\right\}\right] \\ \mathrm{erf(z)} &= \frac{2}{\pi}\int_0^z \exp\left(-t^2\right)dt \end{aligned} \quad (1)$$

B. Auto-correlation of Phase Error

Looking at Fig.2, we see that the frequency error depends on the difference between adjacent samples of the phase error. In order to derive the distribution of the frequency error, we need to know how $\phi(t)$ and $\phi(t-T_u)$ are correlated. The time domain auto-correlation of $\phi(t)$ is therefore important for us. When the auto-correlation function is low, it is an indication that the signals are independent from each other and vice versa. In this paper, we use the frequency spectrum of $\phi(t)$ as a way to analyze its auto-correlation function.

Figure 5 shows the frequency spectrum of the phase error. From Fig.5, we see clearly that the energy is approximately distributed at a frequency bandwidth of 2,400 Hz. The attenuated energies outside 2,400 Hz is also noticeable from the figure. Originally, the noise from the receiver is modeled as a white noise. However, when band limitation is done with the filter of receiver, the noise frequency spectrum follows the band limitation filter. We can therefore say that the phase error

is also a colored noise following the receiver filter spectrum.

From the Wiener-Khintchine theorem [7], it is a common knowledge the auto-correlation function of white noise is a delta function. The Wiener-Khintchine theorem which shows the relationship of the power spectrum and the correlation function is given in eq.(2). Using the inverse Fourier transform of the power spectrum density $|\Phi(\omega)|^2$, it is possible to calculate correlation function $\alpha(\tau)$.

$$\alpha(\tau) = \int_{-\infty}^{\infty} |\Phi(\omega)|^2 \exp(j\omega\tau) d\omega \tag{2}$$

Since the filtering was done in the receiver, the auto-correlation of the phase error now changes to eq.(2). It can be shown that for the box receiver filter the resulting auto-correlation function of a filtered white noise is eq.(3) where B is filter bandwidth, f_0 is the carrier frequency, and σ^2 is the energy of noise, respectively.

$$\alpha(\tau) = B\sigma^2 \frac{\sin(\pi B\tau)}{\phi B\tau} \cos(2\pi f_0 \tau) \tag{3}$$

Based on eq.(3), we plot the resulting auto-correlation function in Fig.6. We see clearly from Fig.6 that this is not a delta function. Because, $\phi(t)$ will have the same characteristic, we conclude that $\phi(t)$ also has the same non-impulsive auto-correlation function and hence $\phi(t)$ and $\phi(t - T_u)$ are correlated.

Now consider a system where up sampling is done on transmitter and band-limitation is done in the receiver. When band limitation using a filter is done, say for a sampling time T_u, correlation occurs as we have shown above. However, depending on the sampling time of the auto-correlation function, the amount of correlation changes. For example, if the sampling rate of the auto-correlation is equal or less than the receiver filter bandwidth, auto-correlation is zero. But as we previously mentioned, we compute the auto-correlation at the up sampled rate making the relationship of $\alpha(0)$ and $\alpha(T_u)$ important for our analysis.

Let β be the coefficient of correlation defined in eq.(4). This coefficient is necessary in order to derive the probability density function of the frequency error. Note that the value of the coefficient of correlation does not depend on SNR. However, it changes depending on frequency bandwidth and sampling time.

$$\beta = \alpha(T_u)/\alpha(0) \qquad (-1 \leq \beta \leq 1) \tag{4}$$

C. Frequency Error

In this part, we examine the probability density function of the frequency error $e(t)$. First, we compare the Gaussian distribution and distribution of of simulated $e(t)$ data. Linear receivers often have error distribution that can be modeled as a Gaussian distribution. But as shown in Fig.7, the Gaussian distribution model does not fit well with the distribution of simulated $e(t)$ data. Hence, we need to derive the desired distribution mathematically.

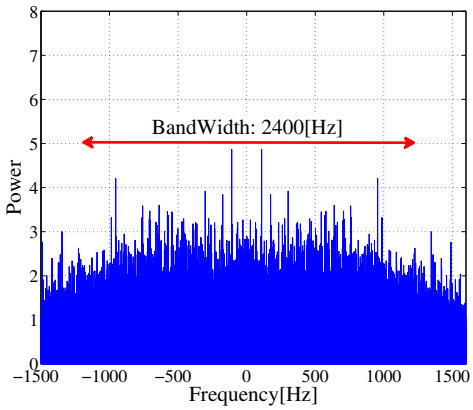

Fig. 5. Frequency Spectrum of Phase Error

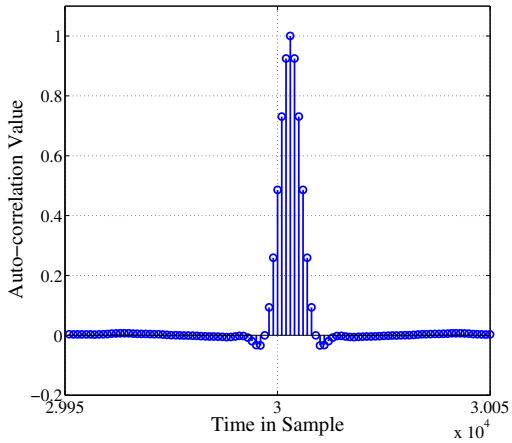

Fig. 6. Auto-correlation of Phase Error

Equation (5) shows the correlation of $\phi(t)$ and $\phi(t - T_u)$.

$$\begin{aligned} \frac{1}{N}\sum_{n=0}^{N-1} \phi(t)^*\phi(t) &= 1 \\ \frac{1}{N}\sum_{n=0}^{N-1} \phi(t-T_u)^*\phi(t-T_u) &= 1 \\ \frac{1}{N}\sum_{n=0}^{N-1} \phi(t)^*\phi(t-T_u) &= \beta \end{aligned} \tag{5}$$

We now define a new random variable δ such that eq.(6) is true. Note that ϕ and δ are independent. In fact, we can think of δ as the reason why $\phi(t)$ and $\phi(t-T_u)$ are not 100% correlated. β on the other hand fixes the correlation of $\phi(t)$ and $\phi(t - T_u)$ [8]. When sampling time between the signals is increased, correlation between the signals disappears and β decreases. And when β is small, the influence of the random variable ϕ also decreases and the random variable ϕ_{T_u} is now mostly dictated by δ. In this case, we can safely say, that like $\phi(t)$ and $\phi(t - T_u)$, δ also has a Nakagami-Rice probability

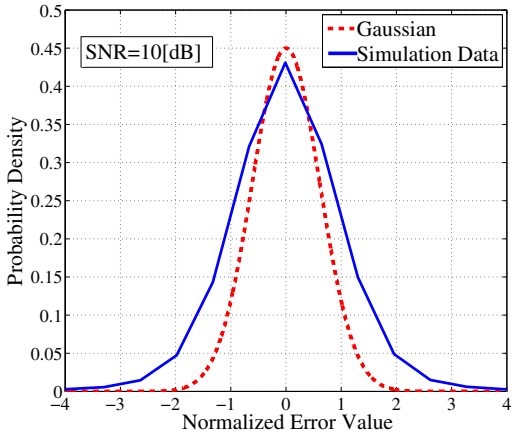

Fig. 7. Comparison of Gaussian Distribution with Simulation Data

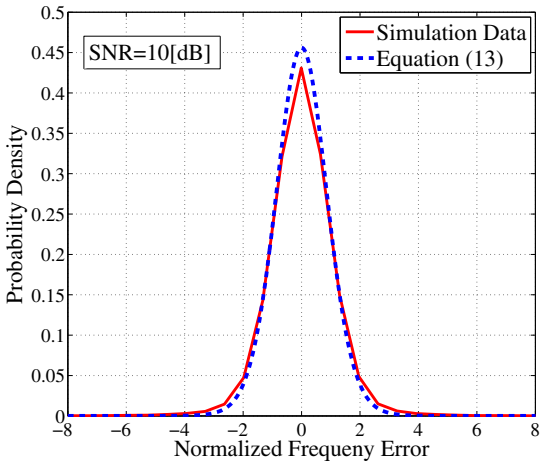

Fig. 8. Comparison of Simulation Data with Equation (13) (SNR = 10 [dB])

distribution.

$$\phi_{T_u} = \beta\phi + \sqrt{1-\beta^2}\delta \tag{6}$$

The frequency error represented as e is calculated from the finite difference of $\phi(t)$ and $\phi(t-T_u)$. This is shown in eq.(7).

$$e = \phi - \phi_{T_u} = (1-\beta)\phi - \sqrt{1-\beta^2}\delta \tag{7}$$

Again, we apply change in variables in eq.(8).

$$\begin{aligned} e &= (1-\beta)\phi - \sqrt{1-\beta^2}\delta \\ u &= \phi \end{aligned} \tag{8}$$

Now let the joint probability density function of e and u be $\psi(e,u)$. Correspondingly, the marginal distribution of e is represented as $g(e)$. Finally, the probability density function $g(e)$ is shown in eq.(9) [9].

$$g(e) = \int_{-\infty}^{\infty} \psi(e(\phi,\delta), u(\phi,\delta))du \tag{9}$$

From eq.(8), solving for random variable ϕ and δ, we get eq.(10).

$$\begin{aligned} \delta &= \frac{1-\beta}{\sqrt{1-\beta^2}}u - \frac{1}{\sqrt{1-\beta^2}}e \\ \phi &= u \end{aligned} \tag{10}$$

In order to solve eq.(9), we use the identity in which employs the Jacobian matrix [10]. This is shown in the equation below.

$$\begin{aligned} J &= \begin{vmatrix} \frac{\partial\delta}{\partial e} & \frac{\partial\delta}{\partial u} \\ \frac{\partial\phi}{\partial e} & \frac{\partial\phi}{\partial u} \end{vmatrix} \\ &= \begin{vmatrix} -\frac{1}{\sqrt{1-\beta^2}} & \frac{1-\beta}{\sqrt{1-\beta^2}} \\ 0 & 1 \end{vmatrix} = \frac{1}{\sqrt{1-\beta^2}} \end{aligned} \tag{11}$$

Because the random variable ϕ and δ are independent, the probability density function can be separated. The probability density function of ϕ is designated as $f_\phi(\phi)$ while the probability density function of δ is designated as $f_\delta(\delta)$. The resulting marginal probability density function of ϕ and δ are then shown in eq.(12).

$$\begin{aligned} g(e) &= \int_{-\infty}^{\infty} f\left(\frac{1-\beta}{\sqrt{1-\beta^2}}\phi - \frac{1}{\sqrt{1-\beta^2}}e, \phi\right)|J|\,d\phi \\ &= \int_{-\infty}^{\infty} f_\delta\left(\frac{1-\beta}{\sqrt{1-\beta^2}}\phi - \frac{e}{\sqrt{1-\beta^2}}\right) f_\phi(\phi)\,\frac{1}{\sqrt{1-\beta^2}}\,d\phi \end{aligned} \tag{12}$$

While we can attempt to evaluate the probability density distribution of frequency error from eq.(13), this is very difficult. We therefore use numerical integration to find the frequency error $e(t)$ probability density function. As shown in Fig.8, the eq.(13) evaluated using numerical integration fits well with the distribution of simulated $e(t)$ data. In Fig.9, the probability density function of each transmitted symbols are superimposed. The regions where probability density functions intersect has a finite probability that it belongs to either of the intersecting functions. The decoding probabilities of signals in these regions are therefore low.

D. LLR for FSK Wireless System

Log likelihood ratio of bit information u_j of the jst transmission symbol u is given by eq.(14) [11].

$$\mathrm{LLR}(u_j) = \log\left(\frac{p(y|u_j=1)}{p(y|u_j=0)}\right) \tag{14}$$

Combining equations (13) and (14), the 0st bit information u_0 and 1st bit information u_1 of transmitted signals u is given by eq.(15).

$$g(e) = \int_{\phi_{min}}^{\phi_{max}} \frac{1}{2\pi} \exp\left(-\frac{1}{2\sigma^2}\right) \left[1 + \sqrt{\frac{\pi}{2}} \frac{\cos\left(\frac{1-\beta}{\sqrt{1-\beta^2}}\phi - \frac{e}{\sqrt{1-\beta^2}}\right)}{\sigma} \exp\left(\frac{\cos^2\left(\frac{1-\beta}{\sqrt{1-\beta^2}}\phi - \frac{e}{\sqrt{1-\beta^2}}\right)}{2\sigma^2}\right) \cdot \left\{1 + \mathrm{erf}\left(\frac{\cos\left(\frac{1-\beta}{\sqrt{1-\beta^2}}\phi - \frac{e}{\sqrt{1-\beta^2}}\right)}{\sqrt{2}\sigma}\right)\right\}\right] \frac{1}{2\pi} \exp\left(-\frac{1}{2\sigma^2}\right) \left[1 + \sqrt{\frac{\pi}{2}} \frac{\cos\phi}{\sigma} \exp\left(\frac{\cos^2\phi}{2\sigma^2}\right) \cdot \left\{1 + \mathrm{erf}\left(\frac{\cos\phi}{\sqrt{2}\sigma}\right)\right\}\right] \frac{1}{\sqrt{1-\beta^2}} d\phi \tag{13}$$

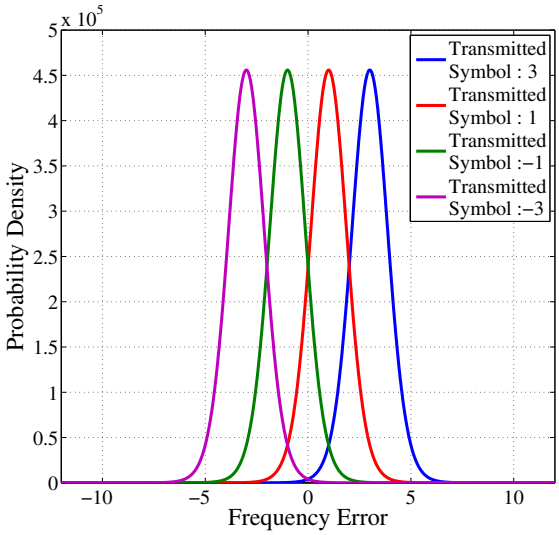

Fig. 9. PDF of Frequency Error of Each Symbol Data (SNR = 10 [dB]))

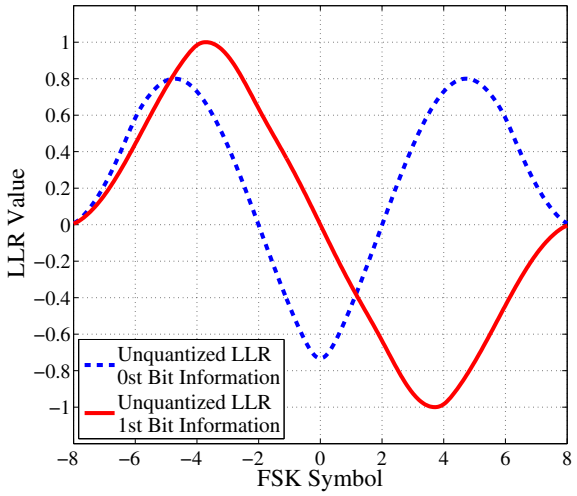

Fig. 10. LLR for FSK Wireless System (SNR = 10 [dB])

$$\begin{aligned} \mathrm{LLR}(u_0) &= \log\left(\frac{g_3(e) + g_{-3}(e)}{g_1(e) + g_{-1}(e)}\right) \\ \mathrm{LLR}(u_1) &= \log\left(\frac{g_{-3}(e) + g_{-1}(e)}{g_3(e) + g_1(e)}\right) \end{aligned} \tag{15}$$

Here, "$g_3(e)$", "$g_1(e)$", "$g_{-1}(e)$", "$g_{-3}(e)$" represents the probability density function of transmission symbols 3, 1, -1 and -3 respectively.

Figure 10 shows the LLR curve according to eq.(15). If the LLR value of the received signal is positive, there is a high probability that the bit value is "1". On the other hand, if the LLR value of the received signal is negative, a high probability that the transmitted bit is "0". The LLR values computed are then passed into the soft decision Viterbi decoder.

IV. Simulation Result

In this part, we did simulation with Rayleigh fading environment. Table II lists the simulation parameters of all environment.

TABLE II
Simulation Parameters

Bit Rate	4.8 [kbps]
Carrier Frequency	467 [MHz]
Coding Rate	2/3
Maximum Doppler Frequency	12.9, 25.8, 32.6, 43.2 [Hz]
Channel	Rayleigh Fading Channel
Number of DATA	400 [bit] (1 [Packet])
Iteration	5000 [times]

11,12,13 and 14, shows the PER characteristic in the cases when the velocity is 30, 60, and 80 km/h respectively. Additionally, Fig.14 shows the PER characteristic in the case when the velocity is 100 km/h.

From Figs.11,12,13 and 14, we see that the case without Viterbi decoder and hard decision Viterbi decoder compared to the case with soft decision Viterbi decoder shows that the latter has improved PER performance. We also see that the PER performance of the uncoded case has a high error floor. On the other hand, we see that the soft decision Viterbi decoder has no visible error floor. Finally, we observe that the 12bit

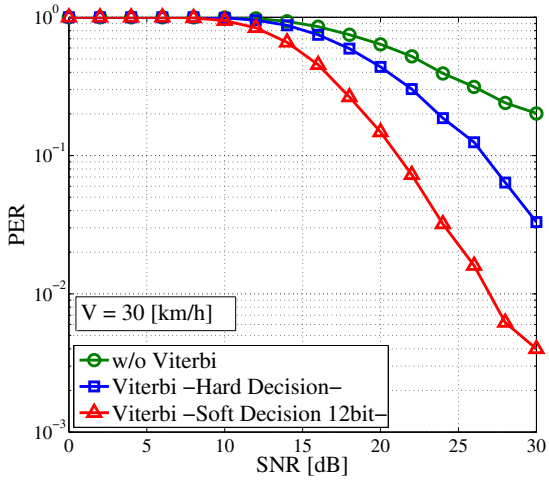

Fig. 11. PER Characteristic (Maximum Doppler Frequency : 12.9 [Hz])

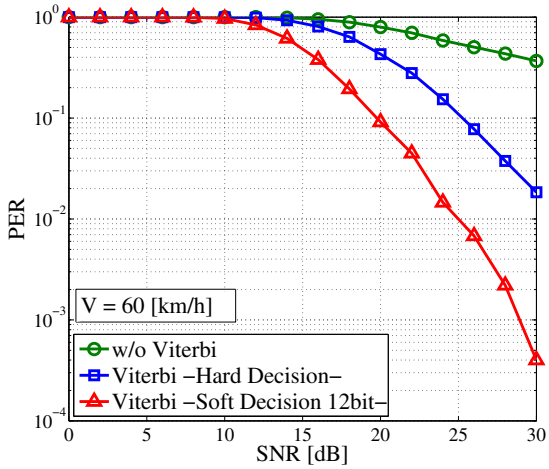

Fig. 12. PER Characteristic (Maximum Doppler Frequency : 25.8 [Hz])

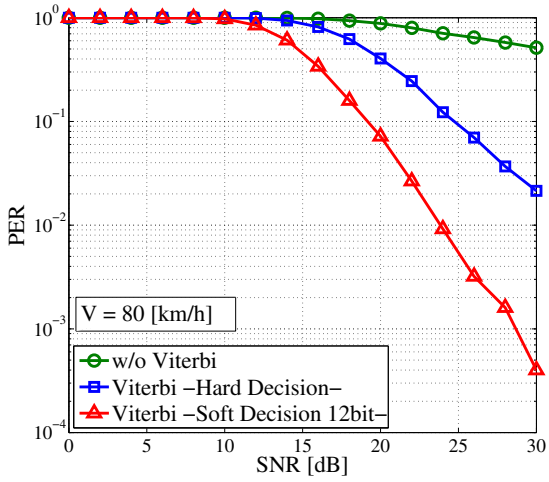

Fig. 13. PER Characteristic (Maximum Doppler Frequency : 34.6 [Hz])

quantized soft decision Viterbi decoder compared to the hard

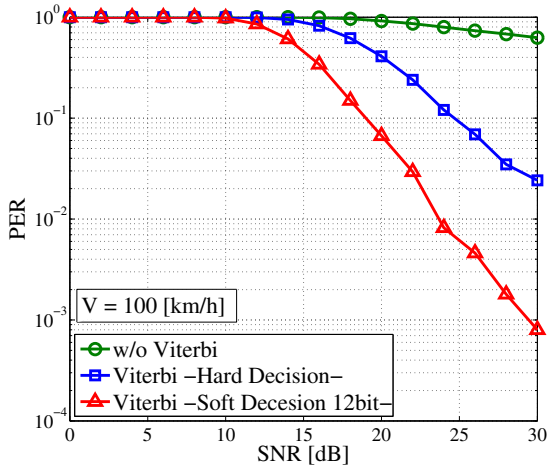

Fig. 14. PER Characteristic (Maximum Doppler Frequency : 43.2 [Hz])

decision Viterbi decoder has at least 5 dB PER performance improvement.

V. Conclusion

In this paper, we have presented a modified LLR which considers the nonlinear characteristic of the frequency discriminator. We have also derived the probability distribution of phase error and frequency error from the output of the frequency discriminator. We have shown through simulations that the phase error follows the Nakagami-Rice distribution. From this, we have formulated the frequency error distribution. By using numerical integration, we were able to apply this result into the LLR calculation. The simulation results in Rayleigh fading environment confirm that performance is improved by using the soft decision Viterbi decoder using modified LLR.

References

[1] ARIB STD-T98, "Digital convenience radio equipment for simplified service," Association of Radio Industries and Businesses, 2009.

[2] A. J. Viterbi, "Convolutional Codes and Their Performance in Communication Systems," *IEEE Trans.Commun.Tech.*, vol.COM-19, pp.752–772. Oct. 1973.

[3] R. Petrovic and A. F. Molisch, "Reduction of multipath effects for FSK with frequency-discriminator detection," in *Proc. PIMRC' 97,* pp.943–948.

[4] Y. Akaiwa and T. Konishi, "An Application of the Viterbi Decoding to Differential Detection of Frequency-Discriminator Demodulated FSK Signal," Proc. The Fourtth International Conference on Personal Indoor and Mobile Radio Communications, pp.210–213.

[5] J. D. Parsons, *The Mobile Radio Propagation Channel.* Wiley, 1992.

[6] M. Nakagami, "The m-Distribution a General Formula of Intensity of Rapid Fading," Statistical Methods in Radio Wave Propagation: Proceedings of a Symposium held at the University of California, pp.3–36, Permagon Press, 1960.

[7] L. W. Couch, *Digital and Analog Communications Systems.* Prentice Hall, 2001.

[8] J. Pitman, *Probability: Springer Texts in Statistics.* Springer, 1997.

[9] S. L. Miller and D. G. Childers, *Probability and Random Processes : With Applications to Signal Processing and Communications.* Academic Press, 2004.

[10] M. Spivak, *Calculus On Manifolds: A Modern Approach To Classical Theorems Of Advanced Calculus.* Westview Press, 1971.

[11] J. G. Proakis, *Digital Communications.* McGraw-Hill, 1995.